# An Algebraic Wavenumber Identification (AWI) technique under stochastic conditions

Xuefeng Li[a], Mohamed Ichchou[a,*], Abdelmalek Zine[b], Christophe Droz[c], Noureddine Bouhaddi[d]

[a]*École Centrale de Lyon, Vibroacoustics & Complex Media Research Group, LTDS - CNRS UMR 5513, Écully 69134, France*
[b]*École Centrale de Lyon, Institut Camille Jordan - CNRS UMR 5208, Écully, France*
[c]*Univ. Gustave Eiffel, Inria, COSYS-SII, I4S Team, Rennes, France*
[d]*Univ. Bourgogne Franche-Comté, FEMTO-ST Institute, Department of Applied Mechanics, CNRS/UFC/ENSMM/UTBM, Besançon, France*

**Abstract**

This paper presents an inverse Algebraic Wavenumber Identification (AWI) technique for multi-modal 1D-periodic structures, which can extract complex wavenumbers from steady-state vibration measurements under stochastic conditions. These wave dispersion characteristics provide valuable vibroacoustic indicators for model updating, damage monitoring in operational conditions, or metamaterial design. Wavenumber extraction techniques are highly sensitive to noisy measurements, nonuniform sampling points, or geometrical uncertainties. The proposed formulation relies on algebraic parameters identification to enable the extraction of complex wavenumbers in four scenarios: (a) low Signal Noise Ratio ; (b) small perturbation caused by uncertainties on sampling points' coordinates ; (c) unknown structural periodicity ; (d) nonuniform sampling. This AWI is compared with Inhomogeneous Wave Correlation (IWC) method and INverse COnvolution MEthod (INCOME) to assess the robustness and accuracy of the method.

*Keywords:* Wavenumber identification; Periodic structures; Inverse method; Small perturbation; Signal noise; Nonuniform sampling.

## 1. Introduction

Wavenumber identification of periodic structures has attracted growing attention in signal processing and mechanical engineering. Periodic structures are materials with periodic variations in geometry or material properties, such as composite sandwich panels, stiffener plates, and truss beams used in aircraft and marine. Periodic structures are widely used in structural vibration isolation due to its band gap characteristic [1]. The band gap is a specific frequency range in which elastic waves cannot propagate. It can be analyzed by dispersion relation, which is usually represented as the relationship between wavenumber and frequency. To achieve wavenumber identification of one-dimensional periodic structures, a number of inverse approaches have been developed in the literature [2–10]. Generally, these inverse methods can be divided into two categories: nonlinear family methods and linear Prony family methods.

*Corresponding author at: École Centrale de Lyon. 36, Avenue Guy de Collongue, Écully 69134, France.
*Email address:* mohamed.ichchou@ec-lyon.fr (Mohamed Ichchou )

In nonlinear family methods, Mc Daniel's method and the Inhomogeneous Wave Correlation (IWC) method are two candidates. Mc Daniel et al. [4, 11] developed a bending wavenumber identification method for 1D structures. This method needs to address a nonlinear fitting optimization problem. Thus it suffers from a high computational cost. In [6], IWC was proposed to identify the K-space of an anisotropic partially clamped ribbed panel and also applied to more complex structures by Ichchou and his co-authors [12–16]. IWC has been proved to be robust to signal noise [17, 18] and not be constrained by uniform sampling. However, IWC typically only provides good results when the displacement field contains many wavelengths, resulting in poor performance at low frequencies. In addition, IWC requires solving a nonlinear wavenumber searching problem, leading to an expensive computational cost.

In linear Prony family methods, the first proposal dates back to the work of Prony in [19], where a non-iterative linear parameter identification technique was proposed for solving the exponential fitting problem. Based on the principle of the Prony method, a series of linear Prony family methods were developed. One example is High Resolution Wavenumber Analysis (HRWA) [9, 20] which makes use of a high-resolution signal processing algorithm called Estimation of Signal Parameters via Rotational Invariance Techniques (ESPRIT)[2] to estimate the wavenumber of 1D structures. Another noteworthy approach is INverse COnvolution MEthod (INCOME) recently proposed in [10] where authors reformulated the classic Prony method in convolution framework, allowing us to identify wavenumbers by a convolution kernel. Compared to nonlinear family methods, the linear Prony family methods are well known for their estimation accuracy in perfect conditions and computational efficiency. Moreover, they have a high resolution to extract propagative wavenumbers and evanescent wavenumbers. Unfortunately, these methods suffer from the constraint of uniform sampling and sensitivity to signal noise, especially with a low signal-to-noise ratio (SNR). In addition, for periodic structures, Ribeiro et al. in [21] have verified numerically and experimentally a conclusion: for the Prony method, the sampling interval needs to be an integer multiple of the structural periodicity. Therefore, INCOME is unable to extract the wavenumber when the unit-cell length of the periodic structures is unknown.

In fact, to achieve more realistic identification in practice, it is also inevitable to take into account the impact of uncertainty of measuring points' coordinates on the extracted wavenumber [22]. This uncertainty is very common in experiments. For instance, it can be caused by grid distortion, manipulation error, or geometric uncertainty of structures. The direct consequence of this uncertainty problem is that displacements of the structure cannot match the coordinates of measurement points. In this paper, this uncertainty problem is called the small perturbation problem. The small perturbation is not additive noise, and the resulting measurement error is not only related to the small perturbation of measurement points' coordinates but also connected to the material properties and excitation frequency. Unfortunately, only a few contributions can be found in the available literature to solve this problem.

To address the drawbacks of the aforementioned inverse methods, this paper proposes a new inverse method called Algebraic Wavenumber Identification (AWI) technique. It is developed based on the algebraic parameter estimator. Over the last few decades, the algebraic parameters estimator for continuous linear time-invariant systems has been proposed by M. Fliess et al. [23–26] and has been theoretically proved to be robust to external signal noise, and structured perturbation [27]. This estimator has been applied to different fields such as vibrating mechanical systems

[28, 29], and nonlinear dynamic systems [30]. In the context of vibroacoustics, a novel formulation for wavenumber extraction is proposed in this paper, making it possible to identify the wavenumber of 1D periodic structures under the following stochastic conditions: a) the high level of external signal noise; b) small perturbation; c) nonuniform sampling; d) the unknown structural periodicity. In detail, the proposed method first uses the algebraic derivative method and Laplace transform to build a linear differential equation with unknown parameters in the wavenumber domain based on a set of discrete noisy data. Then, an exact formula with the multiple integrals over signal is obtained when placed in the spatial domain using operational calculus transform. Finally, the unknown parameters are solved by using the least-squares method. It is worth noting that the introduction of multiple integrals improves the robustness of AWI to different measurement errors. Moreover, AWI treats the signal as a continuous function, freeing it from specific sampling limitations. The highlights of the proposed method are summarized as follows:

- The proposed method allows extracting the wavenumber of 1D periodic structures over the whole frequency range under stochastic conditions, overcoming the drawbacks of other inverse methods, such as INCOME and IWC.
- The proposed method is the first to draw inspiration from the algebraic parameters estimator for wavenumber identification of periodic structures.
- The proposed method has a high resolution to extract propagative wavenumbers and evanescent wavenumbers. Moreover, it can provide wavenumbers with high precision in perfect condition.
- The proposed method only needs to solve small linear problems, thus having a low computational cost.

The rest of this paper is organized as follows: In Section 2, a stochastic signal model for the beam is firstly presented, then the formulation of AWI is derived in detail. This is followed by a series of numerical cases to verify the advantages of AWI over INCOME and IWC. In Section 4, an experimental study is carried out to test the sensitivity of the AWI and IWC to the samples in the vicinity of structural discontinuities. Some conclusions are presented in Section 5.

## 2. Algebraic Wavenumber Identification (AWI)

This section aims to introduce the theory behind the Algebraic Wavenumber Identification (AWI) technique. First, a stochastic signal model of the beam in the presence of small perturbation is established in Section 2.1. Then, in Section 2.2, the fundamental principle of AWI is derived for the case where a single plane wave propagates in the beam. Section 2.3 provides the formula for the general case where multiple waves are present. Finally, AWI implementation is introduced in Section 2.4.

### 2.1. *Stochastic signal model of a beam in the presence of small perturbation*

The general analytical solution of the transverse displacement for a beam such as the EB beam or periodic beam at each angular frequency $\omega$ can be expressed [31] as:

$$U(x_n) = A_1 e^{-ikx_n} + A_2 e^{ikx_n} + A_3 e^{-kx_n} + A_4 e^{kx_n} \tag{1}$$

where the first two terms are the propagative waves propagating in positive and negative directions, and the second two terms are evanescent waves, amplitudes of which decrease exponentially with distance. Evanescent waves exist in structural discontinuities, such as near boundaries or localized excitation sources. Therefore, they are also referred to as "near fields". Eq. (1) can also be rewritten as:

$$U(x_n) = \sum_{m=1}^{4} A_m e^{p_m x_n} \tag{2}$$

where $p_1$=$-ik$, $p_2$= $ik$, $p_3 = -k$, and $p_4 = k$. When multiple waves propagate along the one-dimensional waveguide, the displacement field can be expressed as a sum of exponential functions:

$$U(x_n) = \sum_{m=1}^{n_w} A_m e^{p_m x_n} \tag{3}$$

where $n_w$ is the number of waves. $A_m$ is unknown complex amplitude of $m^{th}$ wave and $p_m$ is related to unknown complex wavenumber $k_m$ ($k_m = jp_m$). It can be noted that this is the signal model used in the AWI method in the perfect condition, which takes into account the propagative waves and evanescent waves.

To build a realistic signal model, it is inevitable to consider measurement points' uncertainty except for external signal noise. In the probabilistic framework, geometric variability of measurement points' coordinates can be quantified by introducing the random variable into each point's coordinate. Thus, the coordinate of the measurement point can be expressed as:

$$\hat{x_n} = x_n(1 \pm \delta_n), \qquad n = 1, ..., N \tag{4}$$

where $N$ is the number of measurement points. $x_n$ is perfect coordinate of $n^{th}$ measurement point. $\delta_n$ is a random variable called the small perturbation ratio, which obeys uniform distribution. Therefore, a stochastic signal model is expressed as:

$$U(\hat{x_n}) = \sum_{m=1}^{n_w} A_m e^{p_m \hat{x_n}} = \sum_{m=1}^{n_w} A_m e^{p_m x_n (1 \pm \delta_n)} \tag{5}$$

To illustrate the measurement error caused by small perturbation, the first-order Taylor expansion of the small

perturbation part of Eq. (5) is considered as follows:

$$\begin{aligned}\sum_{m=1}^{n_w} A_m e^{p_m x_n(1\pm\delta_n)} &= \sum_{m=1}^{n_w} A_m e^{p_m x_n}(1 \pm p_m x_n \delta_n + o(x_n^2\delta_n^2)) \\ &\approx \sum_{m=1}^{n_w} A_m e^{p_m x_n} \pm A_m e^{p_m x_n} p_m x_n \delta_n \end{aligned} \tag{6}$$

where $A_m e^{p_m x_n}$ is unperturbed part and $\pm A_m e^{p_m x_n} p_m x_n \delta_n$ is perturbed part. The latter part consists of three influence factors that lead to the measurement errors: small perturbation ratio $\delta_n$ and pairwise unknown parameters $\{A_m, p_m\}_{m=1}^{n_w}$ which are related to the material properties and excitation frequency. Since the coordinates $\hat{x_n}$ of small perturbed samples are unknown in practice, the coordinate of each measurement point is represented by corresponding unperturbed coordinates $x_n$. Therefore, $U(\hat{x_n})$ can be represented by $S(x_n)$ in the next sections for uniformity of coordinate notation.

### 2.2. *Fundamental principle (one wave case)*

Firstly, the problem formula is proposed. When only one wave propagating in a given direction along the beam is considered, the displacement field in small perturbation condition can be expressed as:

$$S(x_n) = U(\hat{x_n}) = Ae^{p\hat{x}_n} \tag{7}$$

where $A$ is unknown complex amplitude and $p$ is related to unknown complex wavenumber $k$ ($k = jp$). The identification of the parameter $k$ is the aim of AWI in this case.

Secondly, a linear differential equation is established in the wavenumber domain. The Laplace transform of signal in Eq. (7) in the wavenumber domain is given by:

$$S(s) = \frac{A}{s - p} \tag{8}$$

A characteristic polynomial is defined as:

$$\Psi(s) = s - p = \sum_{i=0}^{1} \gamma(1-i)s^i = \gamma(1) + \gamma(0)s \tag{9}$$

where $\gamma(0)$ and $\gamma(1)$ are unknown coefficients of the characteristic polynomial. When $\gamma(0)$ equals to -1, the $\gamma(1)$ will equal to unknown parameter $p$. Multiplying out the Eq. (8) by Eq. (9), one can obtain:

$$S(s)\Psi(s) = \frac{A}{s - p}(s - p) = A \tag{10}$$

A differential equation can be established by taking the derivative of Eq. (10) with respect to $s$ one time:

$$\frac{\mathrm{d}\left(S(s)\Psi(s)\right)}{\mathrm{d}s} = 0 \tag{11}$$

Taking Eq. (9) into Eq. (11) and according to the basic property[1] of algebraic derivative, we can obtain:

$$\begin{aligned}\frac{\mathrm{d}\left(S(s)\Psi(s)\right)}{\mathrm{d}s} &= \frac{\mathrm{d}\left[(\gamma(1)+\gamma(0)s)S(s)\right]}{\mathrm{d}s} \\ &= \gamma(1)\frac{\mathrm{d}S(s)}{\mathrm{d}s} + \gamma(0)S(s) + \gamma(0)s\frac{\mathrm{d}S(s)}{\mathrm{d}s} \\ &= 0\end{aligned} \tag{12}$$

To eliminate derivations operation in the spatial domain, dividing Eq. (12) by $s^2$:

$$\frac{\gamma(1)}{s^2}\frac{\mathrm{d}S(s)}{\mathrm{d}s} + \frac{\gamma(0)}{s}\frac{\mathrm{d}S(s)}{\mathrm{d}s} + \frac{\gamma(0)}{s^2}S(s) = 0 \tag{13}$$

It is noted that AWI treats the displacement field as a continuous function, allowing the extraction of wavenumbers from any sampling way.

Thirdly, Eq. (13) is turned to the spatial domain. Applying operational calculus rules [2] [32, 33] to each term of Eq. (13), an exact formula in the spatial domain can be obtained as follows, after rearrangement:

$$-\gamma(1)\int_0^{x_n}\int_0^{\tau_1}\tau_2 S(\tau_2)\mathrm{d}\tau_2\mathrm{d}\tau_1 - \gamma(0)\int_0^{x_n}\tau_1 S(\tau_1)\mathrm{d}\tau_1 + \gamma(0)\int_0^{x_n}\int_0^{\tau_1} S(\tau_2)\mathrm{d}\tau_2\mathrm{d}\tau_1 = 0 \tag{14}$$

In order to simplify the expression of Eq. (14), the following equations can be obtained by using integral notation [3] [27]:

$$\gamma(1)\int^{(2)} x_n S(x_n) - \gamma(0)\left(\int^{(2)} S(x_n) - \int^{(1)} x_n S(x_n)\right) = 0 \tag{15}$$

[1] $\frac{\mathrm{d}}{\mathrm{d}s}(f\times g) = g\frac{\mathrm{d}f}{\mathrm{d}s} + f\frac{\mathrm{d}g}{\mathrm{d}s}$

[2] Let $\zeta$ denote the usual operational calculus transform acting on signal. Recall that $\zeta^{-1}\left(\frac{\mathrm{d}^\alpha S(s)}{\mathrm{d}s^\alpha}\right) = (-1)^\alpha \tau^\alpha S(\tau)$ and $\zeta^{-1}\left(\frac{S(s)}{s^\alpha}\right) = \int_0^{x_n}\int_0^{\tau_1}\int_0^{\tau_2}\cdots\int_0^{\tau_{\alpha-1}} S(\tau_\alpha)\mathrm{d}\tau_\alpha\ldots\mathrm{d}\tau_2\mathrm{d}\tau_1$

[3] We have donated by $\int^{(\alpha)} S(x_n)$ the quantity $\int_0^{x_n}\int_0^{\tau_1}\int_0^{\tau_2}\cdots\int_0^{\tau_{\alpha-1}} S(\tau_\alpha)\mathrm{d}\tau_\alpha\ldots\mathrm{d}\tau_2\mathrm{d}\tau_1$. Moreover, $\int^{(1)} S(x_n) = \int S(x_n) = \int_0^{x_n} S(\tau_1)\mathrm{d}\tau_1$

It is noted that the introduction of multiple integrals improves the robustness of AWI to the large measurement errors since the multiple integrals operate like a low pass filter [34]. Eq. (15) is hold for each sample. Thus, the linear system of equations can be obtained:

$$\gamma(1)\phi(1, x_n) - \gamma(0)\phi(0, x_n) = 0, \qquad n = 1, ..., N \tag{16}$$

with

$$\phi(1, x_n) = \int^{(2)} x_n S(x_n), \qquad \phi(0, x_n) = \int^{(2)} S(x_n) - \int^{(1)} x_n S(x_n)$$

Finally, the complex wavenumber is estimated using the least squares method. Eq. (16) can be expressed in the matrix format:

$$H_1 X_1 = 0 \tag{17}$$

with

$$H_1 = \begin{bmatrix} \phi(1, x_1) & \phi(0, x_1) \\ \phi(1, x_2) & \phi(0, x_2) \\ \vdots & \vdots \\ \phi(1, x_N) & \phi(0, x_N) \end{bmatrix}, \qquad X_1 = \begin{bmatrix} \gamma(1) \\ \gamma(0) \end{bmatrix}$$

In this context, the unknown parameter $p$ can be estimated by means of the least squares method:

$$\begin{cases} X_1 = argmin\{x^* H_1^* H_1 x\} \\ p = -\frac{\gamma(1)}{\gamma(0)} \end{cases} \tag{18}$$

where $X_1$ is the eigenvector corresponding to the smallest eigenvalue of $H_1^* H_1$. Finally, the wavenumber $k$ can be obtained by:

$$k = jp \tag{19}$$

It is important to note that for the linear Prony family methods, the roots obtained from the characteristic polynomial are propagation constants $\lambda$. Thus the wavenumber can be obtained by using $k = jln\lambda/\Delta x$ where $\Delta x$ is the periodic sampling interval. In contrast, the wavenumber of AWI is obtained directly from the roots of the characteristic polynomial Eq. (9), making it free of the periodic sampling constraint.

### 2.3. General formulation (multiple waves case)

Firstly, the problem formula is proposed. In this section, we consider the general case where the stochastic displacement field is comprised of multiple waves and their reflections as follows:

$$S(x_n) = U(\hat{x_n}) = \sum_{m=1}^{n_w} A_m e^{p_m \hat{x_n}} \tag{20}$$

where $p_m$ is related to unknown complex wavenumber $k_m$ ($k_m = jp_m$) of $m^{th}$ wave. AWI aims to extract complex wavenumbers of all types of waves, including propagative waves and evanescent waves.

Secondly, a linear differential equation is established in the wavenumber domain. A new collection of harmonic responses can be obtained by computing the Laplace transform of $S(x_n)$ in the wavenumber domain:

$$S(s) = \frac{A_1}{s - p_1} + \frac{A_2}{s - p_2} + \cdots + \frac{A_{n_w}}{s - p_{n_w}} \tag{21}$$

The corresponding characteristic polynomial in the wavenumber domain is defined as:

$$\Psi(s) = \prod_{m=1}^{n_w}(s - p_m) = \sum_{i=0}^{n_w} \gamma(n_w - i)s^i \tag{22}$$

where $\gamma(n_w - i)_{\{i\in[0,n_w]\}}$ are coefficients of characteristic polynomial and each coefficient is an elementary symmetric polynomial related to $\{p_1, p_2 \cdots p_{n_w}\}$. Therefore, a new function in the wavenumber domain is expressed by multiplying Eq. (21) and Eq. (22):

$$\begin{aligned} S(s)\Psi(s) &= \left(\frac{A_1}{s - p_1} + \frac{A_2}{s - p_2} \cdots + \frac{A_{n_w}}{s - p_{n_w}}\right) \times \prod_{m=1}^{n_w}(s - p_m) \\ &= A_1(s - p_2)(s - p_3)\cdots(s - p_{n_w}) + \cdots + A_{n_w}(s - p_1)(s - p_2)\cdots(s - p_{n_w-1}) \\ &= \sum_{m=1}^{n_w} A_m \prod_{i=1, i\neq m}^{n_w} (s - p_i) \end{aligned} \tag{23}$$

As seen in Eq. (23), the highest order of the function $S(s)\Psi(s)$ is $n_w - 1$, thus the following equation can be obtained by differentiating Eq. (23) $n_w$ times:

$$\frac{\mathrm{d}^{n_w}\left(S(s)\Psi(s)\right)}{\mathrm{d}s^{n_w}} = \frac{\mathrm{d}^{n_w}\left(S(s)\sum_{i=0}^{n_w}\gamma(n_w - i)s^i\right)}{\mathrm{d}s^{n_w}} = 0 \tag{24}$$

To calculate Eq. (24) easily, the following formulas are introduced:

- Leibniz formula:

$$\frac{\mathrm{d}^n\left(S(s)\Psi(s)\right)}{\mathrm{d}s^n}=\sum_{j=0}^{n}\binom{n}{j}\frac{\mathrm{d}^{n-j}(S(s))}{\mathrm{d}s^{n-j}}\frac{\mathrm{d}^j(\Psi(s))}{\mathrm{d}s^j}$$

- *nth*-order derivative of the wavenumber function $s^l$:

$$\frac{\mathrm{d}^n(s^l)}{\mathrm{d}s^n}=\begin{cases}\dfrac{l!}{(l-n)!}s^{l-n} \quad ; & 0<n\leq l\\ 0 \quad ; & 0<l<n\\ \dfrac{(-1)^n(n-l-1)!}{(-l-1)!}s^{l-n} \quad ; & l<0<n\end{cases}$$

where $n:1,2,3\cdots,n_w$, $\binom{f}{h}=f!/(h!(f-h)!)$ denotes combination number formula.

Based on the formulas above, the following equation can be obtained easily:

$$\frac{\mathrm{d}^{n_w}\left(s^iS(s)\right)}{\mathrm{d}s^{n_w}}=s^{i-n_w}\sum_{j=0}^{n_w}\frac{\mathrm{d}^jS(s)}{\mathrm{d}s^j}s^j\binom{i}{n_w-j}(n_w-j)!\binom{n_w}{j} \tag{25}$$

In this context, a linear differential equation can be established by combining Eq. (24) and Eq. (25):

$$\sum_{i=0}^{n_w}\sum_{j=i}^{n_w}\binom{n_w}{j}\binom{n_w-i}{n_w-j}(n_w-j)!s^{j-i}\frac{\mathrm{d}^jS(s)}{\mathrm{d}s^j}\gamma(i)=0 \tag{26}$$

Similar to one wave case, dividing Eq. (26) by $s^{n_w+1}$ can eliminate derivations operation and guarantee that each term containing the signal $S(x_n)$ will be affected by at least an integral in the spatial domain. Thus, the following equation can be obtained:

$$\sum_{i=0}^{n_w}\sum_{j=i}^{n_w}\binom{n_w}{j}\binom{n_w-i}{n_w-j}(n_w-j)!\frac{1}{s^{n_w+1+i-j}}\frac{\mathrm{d}^jS(s)}{\mathrm{d}s^j}\gamma(i)=0 \tag{27}$$

Thirdly, Eq. (27) is turned to the spatial domain. The operational calculus transform is applied to the following part of the Eq. (27):

$$\sum_{j=i}^{n_w}\frac{1}{s^{n_w+1+i-j}}\frac{\mathrm{d}^jS(s)}{\mathrm{d}s^j}=\int^{(n_w+1+i-j)}(-1)^jx_n^jS(x_n) \tag{28}$$

Thus, the following formula can be obtained by incorporating Eq. (28) into Eq. (27):

$$\sum_{i=0}^{n_w} \phi(i, x_n)\gamma(i) = 0 \tag{29}$$

with

$$\phi(i, x_n) = \sum_{j=i}^{n_w} \binom{n_w}{j}\binom{n_w - i}{n_w - j}(n_w - j)! \times \left( \int^{(n_w+1+i-j)} (-1)^j x_n^j S(x_n) \right)$$

where $\int^{(n_w+1+i-j)} (-1)^j x_n^j S(x_n)$ is a multiple integral [35] which is applied to filter the signal with large measurement errors and attenuate the effects of high-frequency noise that is probably present in measurements.

Finally, the complex wavenumber is estimated using the least squares method. Eq. (29) can be expressed in the matrix form:

$$HX = 0 \tag{30}$$

with

$$H = \begin{bmatrix} \phi(n_w, x_1) & \phi(n_w - 1, x_1) & \cdots & \phi(0, x_1) \\ \phi(n_w, x_2) & \phi(n_w - 1, x_2) & \cdots & \phi(0, x_2) \\ \vdots & \vdots & \ddots & \vdots \\ \phi(n_w, x_N) & \phi(n_w - 1, x_N) & \cdots & \phi(0, x_N) \end{bmatrix}, \qquad X = \begin{bmatrix} \gamma(n_w) \\ \gamma(n_w - 1) \\ \vdots \\ \gamma(0) \end{bmatrix}$$

The estimation of the coefficients of characteristic polynomial Eq. (22) can be obtained by solving the least squares problem as follows:

$$X = argmin\{x^* H^* H x\} \tag{31}$$

where the vector $X$ is the eigenvector corresponding to the smallest eigenvalue of $H^*H$.

After calculating the roots of the characteristic polynomial Eq. (22), the wavenumbers $k_m$ can be calculated by:

$$k_m = jp_m \tag{32}$$

Note that in any case, one wave case mentioned in Section 2.2 or general case in this section, the fundamental step is to calculate the multiple integrals of coefficients $\phi(i, x_n)$. In this paper, a solution of multiple integrals is proposed as the following process:

In multiple integrals of Eq. (29), the integral function is a product between displacement field $S(x_n)$ and space variable $x_n$. However, our aim is to calculate the multiple integrals of the displacement field. Thus, the first step is to

split space variable $x_n$ from integrals by using the following fact (see [36] ):

$$\int^{(q)} (x_n)^j S(x_n) = \sum_{i=0}^{j} (-1)^i \binom{i+q-1}{q-1} \binom{j}{i} i! x_n^{j-i} \int^{(i+q)} S(x_n) \tag{33}$$

Based on the result of Eq. (33), $\phi(i, x_n)$ of Eq. (29) can be rearranged as:

$$\begin{aligned} \phi(i, x_n) = \sum_{j=i}^{n_w} \sum_{m=0}^{j} (-1)^{m+j} \binom{n_w - i}{n_w - j} \binom{m + n_w + i - j}{n_w + i - j} \binom{n_w}{j - m} (n_w + m - j)! \\ \times x_n^{j-m} \int^{(m+n_w+1+i-j)} S(x_n) \end{aligned} \tag{34}$$

To simplify the above equation, the variable change $m = j - r$ is taken into Eq. (34), and the summation on the index $j$ has the closed form:

$$\sum_{j=i}^{n_w} \binom{n_w - i}{n_w - j} \binom{n_w + i - r}{n_w + i - j} = \frac{(2n_w - r)!}{(n_w - r)!(n_w)!} \tag{35}$$

and the Eq. (34) becomes:

$$\phi(i, x_n) = \sum_{r=0}^{n_w} (-1)^r \frac{(2n_w - r)!}{(n_w - r)! r!} x_n^r \int^{(n_w+i+1-r)} S(x_n) \tag{36}$$

In Eq. (36), the multiple integrals of displacement field $S(x_n)$ can be calculated by the following fact, which is a process of converting multiple integrals into a single integral:

$$\int^{(\alpha)} S(x_n) = \int_0^{x_n} \int_0^{\tau_1} \int_0^{\tau_2} \dots \int_0^{\tau_{\alpha-1}} S(\tau_\alpha) \mathrm{d}\tau_\alpha \dots \mathrm{d}\tau_2 \mathrm{d}\tau_1 = \frac{1}{(\alpha - 1)!} \int_0^{x_n} (x_n - \tau)^{\alpha-1} S(\tau) \mathrm{d}\tau \tag{37}$$

Finally, the following equation can be obtained by combining Eq. (36) and Eq. (37):

$$\phi(i, x_n) = \sum_{r=0}^{n_w} \frac{(-1)^r (2n_w - r)! x_n^r}{(n_w - r)! r! (n_w + i - r)!} \int_0^{x_n} (x_n - \tau)^{n_w+i-r} S(\tau) \mathrm{d}\tau \tag{38}$$

where the single integral can be calculated easily using the numerical integration method. In this paper, the single integral is approximated using the trapezoidal integration method.

### 2.4. AWI implementation

The algorithm of AWI is implemented for each given frequency as follows:

**Algorithm**: Algebraic Wavenumber Identification (AWI) technique

**Set** displacement field, coordinates of measurement points
**For** each frequency $\omega$ **do**
  **For** each displacement $S(x_n)$ **do**
  → Calculate single integral of Eq. (38) using trapezoidal integration method
  → Calculate each element $\phi(i, x_n)$ of a new matrix $H$ (see Eq. (38))
  **End for**
→ Build a new matrix $H$ using $\phi(i, x_n)$ (see Eq. (30))
→ Calculate the coefficients $\gamma(i)$ of characteristic polynomial through least squares method (see Eq. (31))
→ Calculate the roots $p_m$ of characteristic polynomial (see Eq. (22))
→ Calculate wavenumber $k_m$ (see Eq. (32))
**End for**

**Fig. 1.** The implementation for AWI.

## 3. Numerical study and parametric survey

In this section, a series of numerical cases are tested to validate the advantages of AWI compared to INCOME and IWC under perfect and stochastic conditions. For stochastic conditions, we consider that samples are affected by two common stochastic perturbations, including external signal noise and small perturbation. In addition, the sensitivity of the inverse methods to the periodicity of periodic structures is worth investigating. The sensitivity here is manifested in two ways: 1) the performance of inverse methods when the structural periodicity is approximately known; 2) the performance of inverse methods when the structural periodicity is unknown. These phenomena are common in practice. For example, periodic structures encased in other materials and structural damage or deformation will inevitably result in unknown or approximately known structural periodicity. In order to apply AWI to different types of structures, three structures, including a homogeneous beam, a homogeneous beam with distributed TMDs, and a bi-material periodic beam, are considered in this section. The Wave Finite Element Method (WFEM) is seen as the reference, and the Finite Element Method (FEM) is used to calculate transverse displacements in the next numerical cases. The normalised wavenumbers by using $k\Delta x/\pi$ with unit-cell length $\Delta x$ are considered. To facilitate the description of the research content of each numerical case, we have organized three numerical studies in the form of a tree diagram, as shown in Fig. 2, where the content in brackets indicates the methods to be compared.

### 3.1. Numerical study 1: a homogeneous beam

This section is devoted to validating that AWI has a low computational cost and high robustness to signal noise. Section 3.1.1 firstly compares the performance of AWI, INCOME, and IWC on extracting propagative wavenumbers

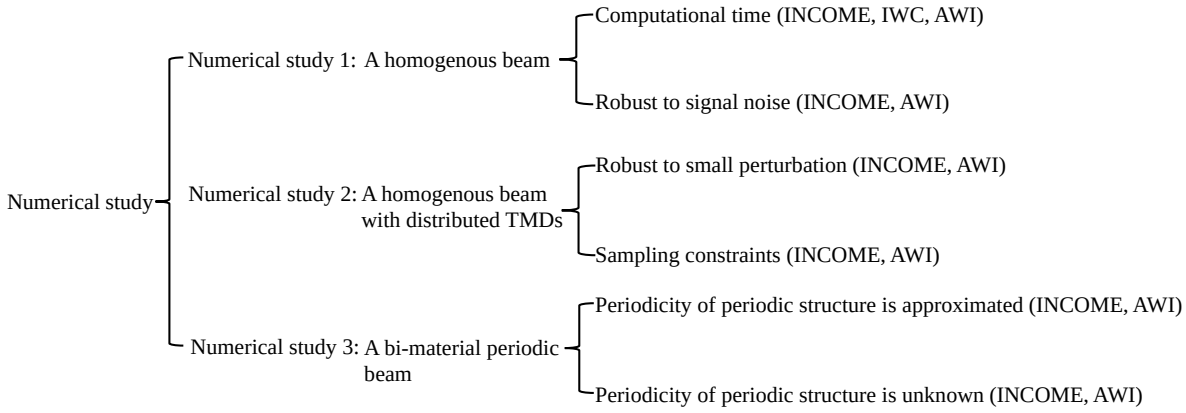


**Fig. 2.** Tree diagram of the numerical study.

and evanescent wavenumbers in perfect condition. Then, the computational costs of these three inverse methods are compared. Comparatively, Section 3.1.2 compares AWI and INCOME under the stochastic condition where forced responses are subjected to high levels of signal noise.

The structure in this section is an aluminum cantilever homogeneous beam that is excited with a force of 10 N at the right end of the beam shown in Fig. 3. The geometrical and material properties are summarized in Table 1.

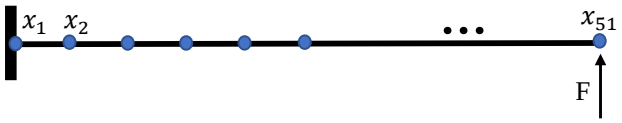


**Fig. 3.** The simulated cantilever homogeneous beam.

**Table 1.** Characteristics of the homogeneous beam.

| Length | Height | Width | Young's modulus | Damping | Poisson's ratio | Density | Force |
|---|---|---|---|---|---|---|---|
| 50 cm | 1 cm | 2 cm | 70 GPa | 2% | 0.3 | 2700 kg/m$^3$ | 10 N |

### *3.1.1. Comparison of computation time*

In this section, three inverse methods are first applied to extract complex wavenumbers using 51 samples (complete data set) in perfect condition. These samples are spaced equally along the whole structure, including the vicinity of the force excitation and boundaries. The resulting dispersion curves for the propagative wave and the evanescent wave are plotted in Fig. 4 (a) and Fig. 4(b), respectively. From these two figures, two observations can be made. First, INCOME, AWI can extract both propagative and evanescent wavenumbers, whereas the IWC can only identify propagative wavenumber. This is because the signal models employed by these inverse methods are different. For INCOME and AWI, the signal is modeled as a sum of exponential functions, as demonstrated by Eq. (3), which includes the propagative waves and evanescent waves. In addition, INCOME and AWI have a high resolution to extract these two types of waves in perfect condition. In contrast, the signal model of IWC, $U(x) = e^{-ikx}$, only considers

propagative waves. Consequently, IWC is unable to identify the evanescent wavenumber. Second, INCOME and AWI can provide complex wavenumbers with high numerical precision in perfect condition. However, the dispersion curves obtained by IWC are characterized by fluctuations, particularly in the low-frequency range. To improve the accuracy of complex wavenumbers obtained by IWC, one way is to avoid using the samples close to the boundaries and force excitations, eliminating the influence of evanescent waves on the propagative wavenumber extraction. In this case, only 41 samples (incomplete data set), excluding 10 samples near the ends of the beam, are used as input parameters of IWC. As shown in Fig. 5 (a), the accuracy of extracted propagative wavenumbers is improved, especially for the imaginary part of wavenumbers. In most cases, the extraction of evanescent waves is not of interest. Thus only propagative wavenumbers are extracted by inverse methods in the following sections.

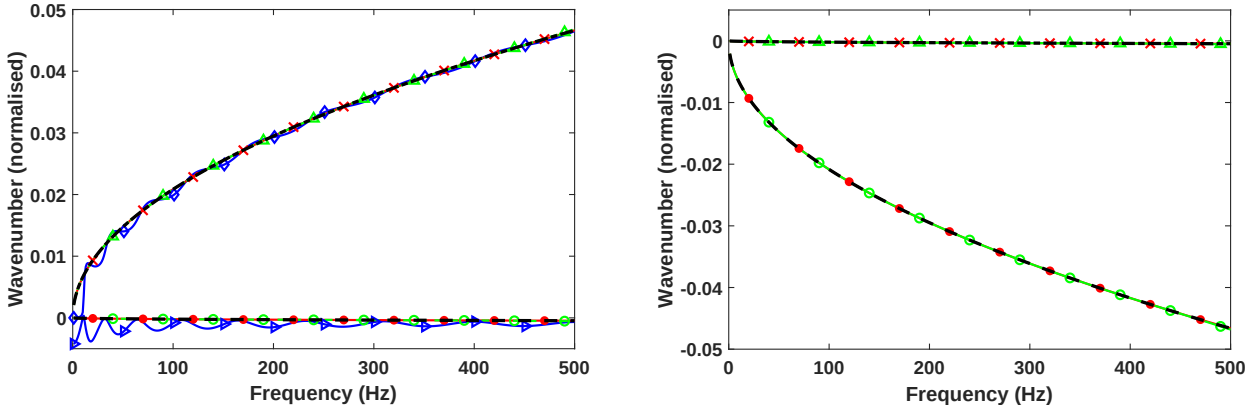


**Fig. 4.** (a) Comparison of propagative wavenumbers obtained by IWC, INCOME, and AWI for a homogeneous beam using complete data set in perfect condition. (b) Comparison of evanescent wavenumbers obtained by INCOME and AWI for a homogeneous beam using complete data set in perfect condition. (◊—) real part of the wavenumber obtained by IWC, (▷—) imaginary part of the wavenumber obtained by IWC, (×—) real part of the wavenumber obtained by INCOME, (•—) imaginary part of the wavenumber obtained by INCOME, (△—) real part of the wavenumber obtained by AWI, (○—) imaginary part of the wavenumber obtained by AWI, (— - —) real part of the wavenumber obtained by WFEM, (- - -) imaginary part of the wavenumber obtained by WFEM.

The computational time of each inverse method is calculated in four steps in this section. The first step is to obtain 10 data sets containing 10, 20, 30, 40, 50, 60, 70, 80, 90, and 100 displacements obtained from the displacement shape at a certain frequency, respectively. The second step is to collect the computational time when each inverse method is performed on these 10 sets of data, respectively. The third step is to repeat the first and the second step at 30 different frequencies. The final step is to average the computation time of each inverse method on these frequency points. The averaged computational time of IWC, INCOME, and AWI is compared in Fig. 5(b). This figure illustrates that AWI and INCOME have lower computational costs than IWC, with AWI being five to eight times faster than IWC.

### *3.1.2. Noise sensitivity*

The experimental samples are often disturbed by external signal noise. Thus we add white gaussian noise to transverse displacements, with a signal-to-noise ratio of 25 in this section. The resulting dispersion curves obtained

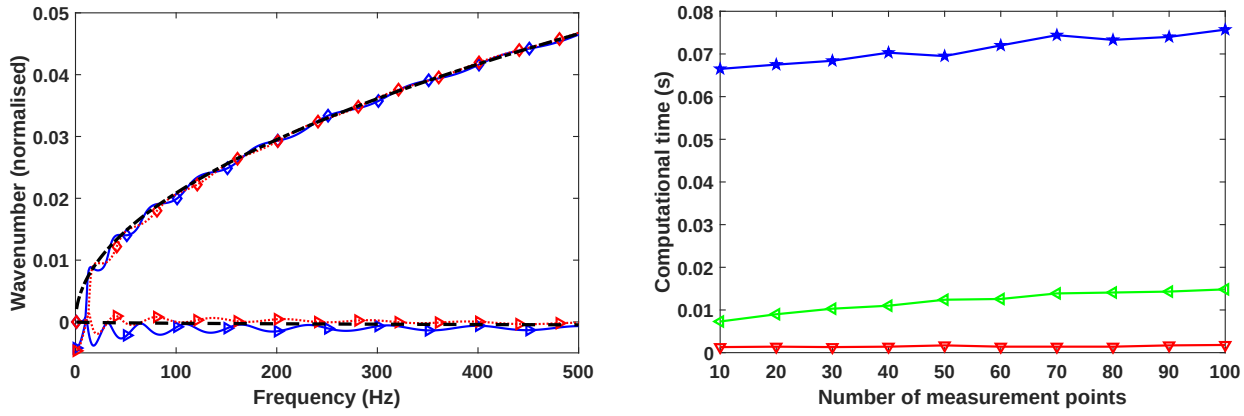


(a) (b)

**Fig. 5.** (a) Comparison of propagative wavenumber obtained by IWC for a homogeneous beam using the complete and incomplete data set in perfect condition, respectively. (◊—) real part of the wavenumber obtained by IWC using the complete data set, (▷—) imaginary part of the wavenumber obtained by IWC using the complete data set, (◊- - - - -) real part of the wavenumber obtained by IWC using the incomplete data set, (▷- - - - -) imaginary part of the wavenumber obtained by IWC using the incomplete data set, (— · —) real part of the wavenumber obtained by WFEM, (- - -) imaginary part of the wavenumber obtained by WFEM. (b) Computational time comparison between IWC, INCOME, and AWI as a function of the measurement points. (★—) computational time of IWC, (▽—) computational time of INCOME, (◁—) computational time of AWI.

by INCOME and AWI are shown in Fig. 6(a) and Fig. 6(b), respectively. From these two figures, two phenomena can be observed. First, AWI is more robust than INCOME. It makes sense because AWI improves the robustness to signal noise by introducing the multiple integrals of the signal. Multiple integrals operate like loss pass filters. Second, INCOME suffers from the problem of yielding complex results when identifying the real part of the wavenumber. This is because the essence of INCOME is the Prony method. As mentioned in [3, 37], the Prony method often produces complex values as the result of estimating real parameters when the signal is affected by high levels of signal noise. Comparatively, AWI does not suffer from such a limitation.

### *3.2. Numerical study 2: a homogeneous beam with Tuned Mass Dampers (TMDs)*

In this section, AWI and INCOME are compared under small perturbation conditions. In Section 3.2.1, the uniform small perturbed samples are selected as input parameters of AWI and INCOME, while the nonuniform small perturbed samples are considered in Section 3.2.2, which also validates that AWI is not limited to uniform sampling. The maximum small perturbation ratio $\delta_n$ is taken as 20% for each measurement point.

The structure in this numerical study is a homogeneous beam with distributed TMDs, as shown in Fig. 7. The host structure is a classical steel beam that is equipped with distributed TMDs, modeled as a mass-spring system. The properties of host beam and TMDs are shown in Table 2 and Table 3 respectively.

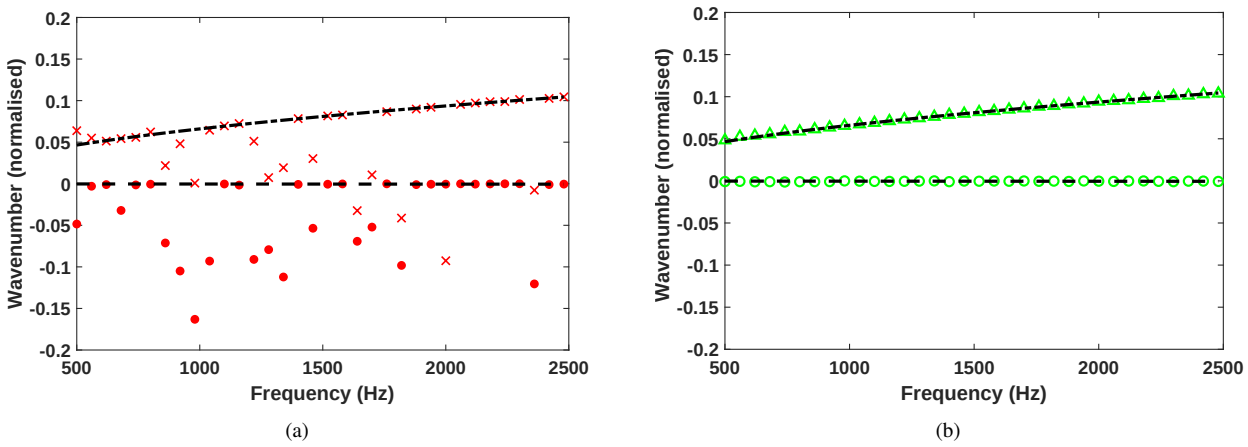


**Fig. 6.** Dispersion curves comparison for a homogeneous beam under signal noise (SNR=25) condition: (a) INCOME and WFEM; (b) AWI and WFEM. (×) real part of the wavenumber obtained by INCOME, (•) imaginary part of the wavenumber obtained by INCOME, (△) real part of the wavenumber obtained by AWI, (○) imaginary part of the wavenumber obtained by AWI, (—·—) real part of the wavenumber obtained by WFEM, (– – –) imaginary part of the wavenumber obtained by WFEM.

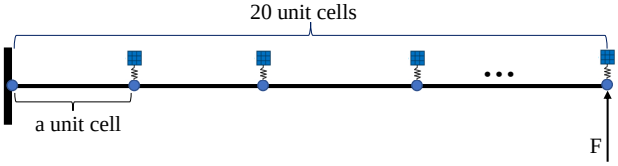


**Fig. 7.** The simulated cantilever homogeneous beam with TMDs.

**Table 2.** Characteristics of the steel host beam.

| Length | Height | Width | Young's modulus | Damping | Poisson ratio | Density | Force |
|---|---|---|---|---|---|---|---|
| 80 cm | 1 cm | 3 cm | 210 GPa | 0.8% | 0.3 | 7900 kg/m$^3$ | 10 N |

**Table 3.** Characteristics of TMD device.

| Number of TMD | Mass ratio | Damping | Resonance frequency |
|---|---|---|---|
| 20 | 2% | 0.5% | 400 Hz |

### *3.2.1. Uniform sampling case under small perturbation condition*

In this case, AWI and INCOME are applied to 81 uniform small perturbed samples. Fig. 8 shows operational deflection shape at 400 Hz. To observe measurement errors caused by the small perturbation problem, we only provide the first 31 displacements. For example, the zoomed sub-picture in Fig. 8 clearly shows the deviation of the disturbed displacements from the corresponding undisturbed displacements for the measurement points at 0.28 m and 0.29 m. The dispersion curves obtained by each method are shown in Fig. 9(a) and Fig. 9(b). Unsurprisingly, there is a good agreement between AWI and WFEM. On the other hand, the band gap from approximately 390 Hz to 410 Hz can be easily identified by AWI. In contrast, INCOME fails to extract wavenumber in this condition, especially in the vicinity

of the band gap where the dispersion curve is featured by big fluctuations.

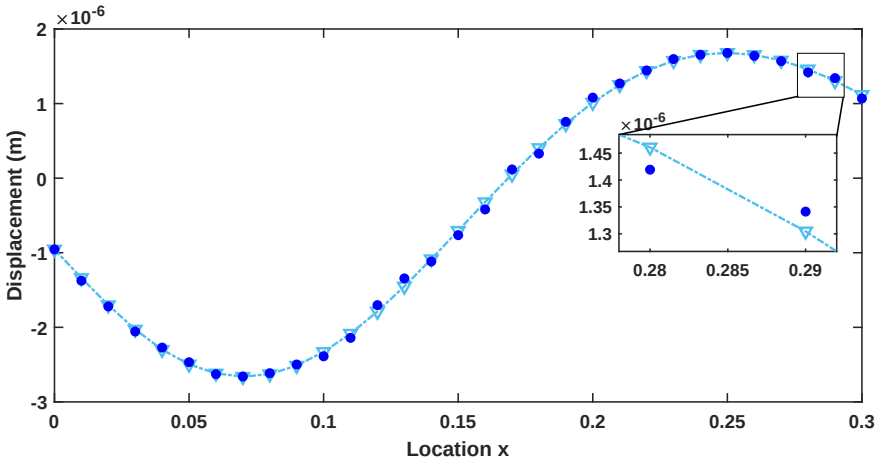


**Fig. 8.** Operational deflection shape at 400Hz. (▽ −·−) uniform perfect samples, (•) uniform small perturbed samples.

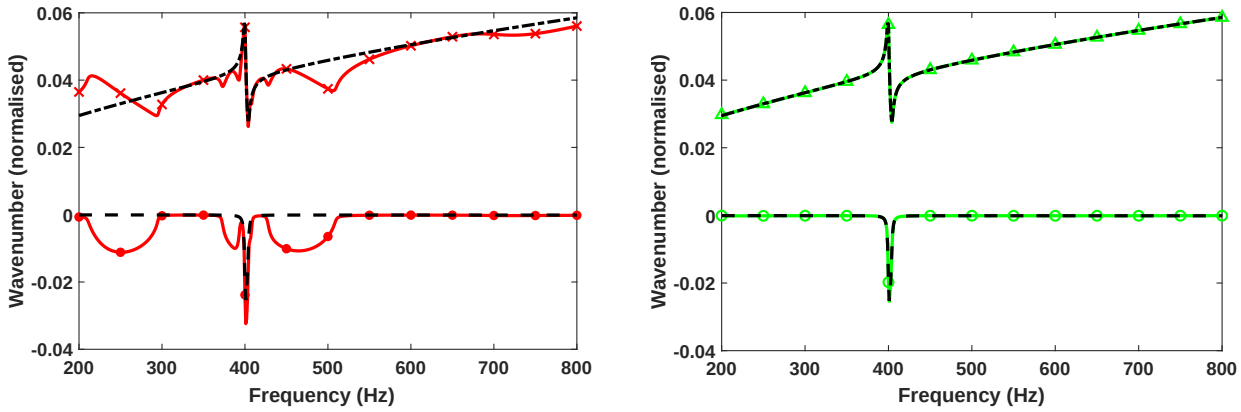


**Fig. 9.** Dispersion curves comparison for a homogeneous beam with distributed TMDs under uniform sampling and small perturbation ($\delta_{max}$ = 20%) condition: (a) INCOME and WFEM; (b) AWI and WFEM. (×—) real part of the wavenumber obtained by INCOME, (•—) imaginary part of the wavenumber obtained by INCOME, (△—) real part of the wavenumber obtained by AWI, (○—) imaginary part of the wavenumber obtained by AWI, (−·−) real part of the wavenumber obtained by WFEM, (– – –) imaginary part of the wavenumber obtained by WFEM.

### *3.2.2. Nonuniform sampling case under small perturbation condition*

In this case, 81 nonuniform small perturbed samples are chosen as input parameters of AWI and INCOME, respectively. For INCOME, to address its limitation of periodic sampling, the cubic spline interpolation is applied to reconstruct uniform samples from nonuniform samples. For example, Fig. 10 shows the displacements of the first 31 measurement points at 500 Hz after using the interpolation strategy. It can be observed that many interpolated samples produce significant displacement errors, such as the points at 0.05 m and 0.06 m, leading to a severely ill-posed problem for INCOME. Consequently, significant deviations between wavenumbers generated by INCOME and those obtained by WFEM exist, as shown in Fig. 11(a). Moreover, this figure indicates that it is difficult to distinguish

the location of the band gap by INCOME in this case. Comparatively, Fig. 11(b), which is the result of AWI, indicates that AWI still performs well on wavenumber identification under this stochastic condition. This is because AWI can identify wavenumbers using nonuniform samples as input parameters, avoiding the use of interpolation strategy, and the introduction of multiple integrals improves the robustness of AWI to large measurement errors.

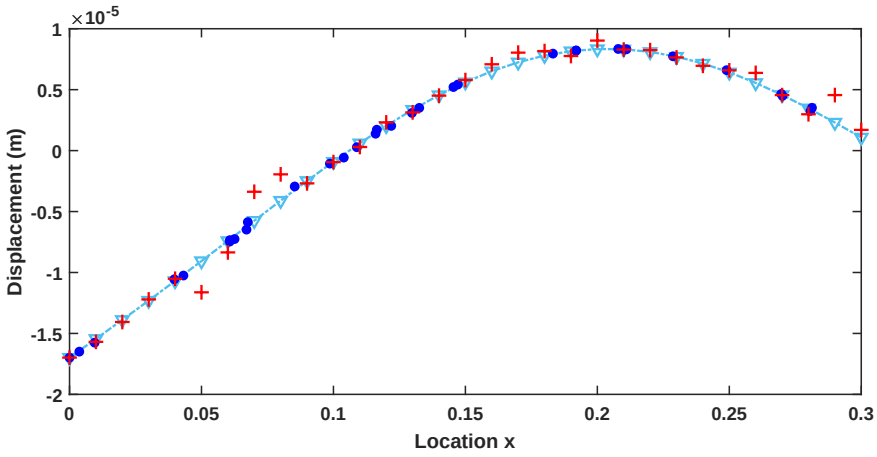


**Fig. 10.** Operational deflection shape at 500 Hz. (▽ — · —) uniform perfect samples, (•) nonuniform small perturbed samples, (+) uniform interpolated samples.

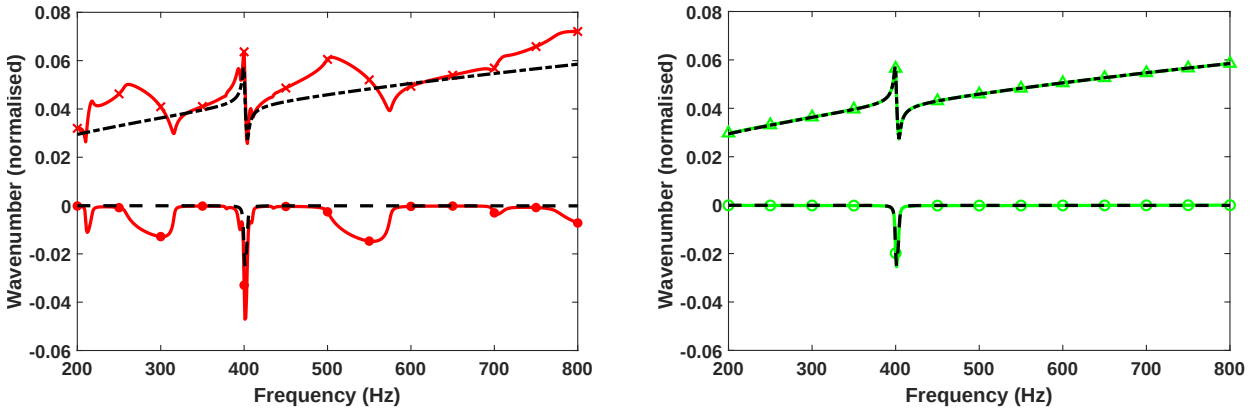


**Fig. 11.** Dispersion curves comparison for a homogeneous beam with distributed TMDs under nonuniform sampling and small perturbation ($\delta_{max}$ = 20%) condition: (a) INCOME and WFEM; (b) AWI and WFEM. (×—) real part of the wavenumber obtained by INCOME, (•—) imaginary part of the wavenumber obtained by INCOME, (△—) real part of the wavenumber obtained by AWI, (○—) imaginary part of the wavenumber obtained by AWI, (— · —) real part of the wavenumber obtained by WFEM, (- - -) imaginary part of the wavenumber obtained by WFEM.

### *3.3. Numerical study 3: a bi-material periodic beam*

To investigate the sensitivity of AWI and INCOME to the periodicity of periodic structures, AWI and INCOME are applied to a bi-material periodic beam composed of 5 unit cells, as shown in Fig. 12 (a). Fig. 12 (b) shows a unit cell composed of two aluminum parts (Young's modulus $E$ = 70 GPa, mass density $\rho$ = 2700 kg/m$^3$, poisson ratio $\nu$

= 0.33, damping $\eta = 0.7\%$). The length and radius of part A are 10 cm and 1 cm, while the length and radius of part 2 are 20 cm and 4 cm. The unit-cell length is 40 cm. In this study, the samples are extracted in the perfect condition for INCOME, while the small perturbed samples with 10% of the maximum small perturbation ratio are considered for AWI.

INCOME requires the sampling interval to be an integer multiple of the periodicity of the periodic structure. Therefore, two cases are worth studying: 1) the approximated periodicity is chosen as 41 cm; 2) the unit-cell length is chosen as 1 cm when the structural periodicity is unknown. Fig. 13 and Fig. 14 present the dispersion curves obtained by INCOME in these two conditions, respectively. Fig. 13 shows that INCOME is unable to extract the accurate dispersion curve even in a perfect condition when only an approximation of structural periodicity is known, while Fig. 14 demonstrates that estimation results are completely wrong when the structural periodicity is unknown. In contrast, AWI has no specific sampling requirements for periodic structures. Therefore, as shown in Fig. 15, when the unit-cell length is unknown, the dispersion curve obtained by AWI agrees well with the result of WFEM, even in the presence of small perturbation.

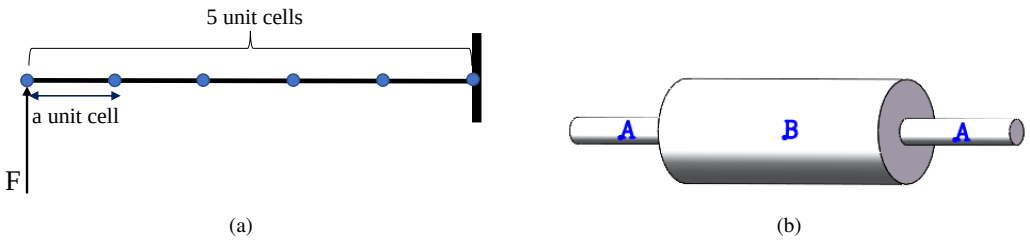


**Fig. 12.** (a) The simulated cantilever bi-material periodic structure, (b) Unit cell.

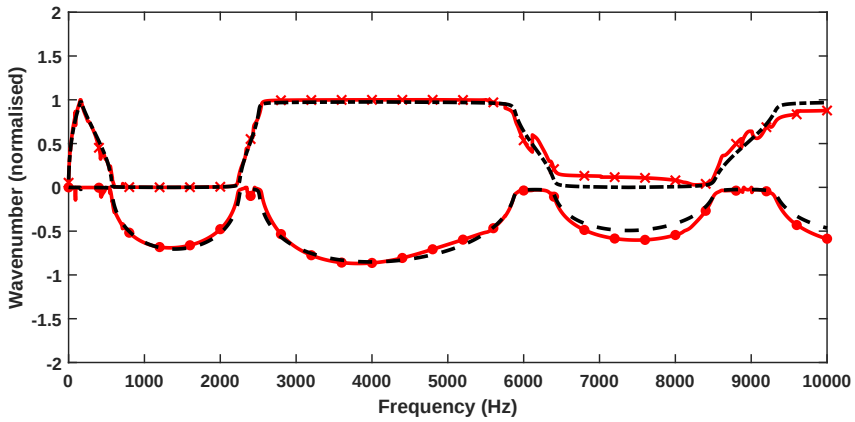


**Fig. 13.** Comparison of dispersion curves obtained by INCOME and WFEM for a bi-material periodic beam under the perfect condition when the unit-cell length is approximated as 41 cm. (×—) real part of the wavenumber obtained by INCOME, (•—) imaginary part of the wavenumber obtained by INCOME, (—·—) real part of the wavenumber obtained by WFEM, (– – –) imaginary part of the wavenumber obtained by WFEM.

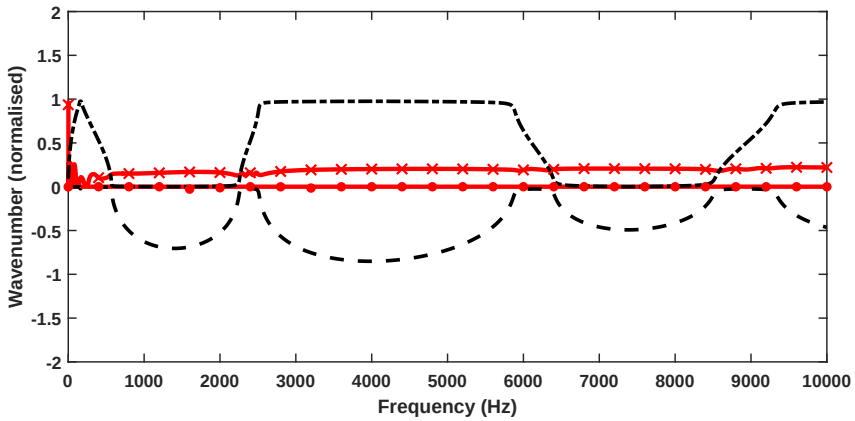


**Fig. 14.** Comparison of dispersion curves obtained by INCOME and WFEM for a bi-material periodic beam under the perfect condition when the unit-cell length is unknown. (×—) real part of the wavenumber obtained by INCOME, (•—) imaginary part of the wavenumber obtained by INCOME, (—·—) real part of the wavenumber obtained by WFEM, (– – –) imaginary part of the wavenumber obtained by WFEM.

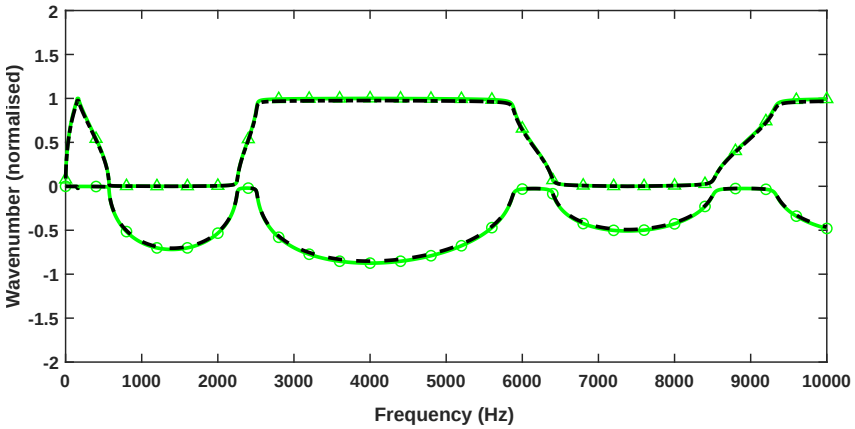


**Fig. 15.** Comparison of dispersion curves obtained by AWI and WFEM for a bi-material periodic beam under small perturbation ($\delta_{max}$ = 10%) condition when the unit-cell length is unknown. (△—) real part of the wavenumber obtained by AWI, (○—) imaginary part of the wavenumber obtained by AWI, (—·—) real part of the wavenumber obtained by WFEM, (– – –) imaginary part of the wavenumber obtained by WFEM.

## 4. Experimental study

In this experimental study, the AWI and IWC are applied to extract the complex wavenumbers of an aluminum beam to investigate their sensitivity to the samples in the structural discontinuities. The tested aluminum beam ($E$ = 79 GPa, $\nu$ = 0.33, $\rho$ = 2700 kg/m$^3$) has the dimensions of 101 cm × 2 cm and the thickness is 1 cm. Fig. 16 presents the experimental set-up for measuring the displacement field. The beam was suspended at the top of a fixed frame and was excited with a white noise by an electrodynamic shaker at the top of the beam. A scanning laser vibrometer was used to measure 200 equally spaced displacements with a 0.5 cm sampling interval. These measured displacements are distributed throughout the structure, including those near the excitation force and the boundaries.

The coherence values for all measurement points are plotted in Fig. 17. The lower the coherence value, the more affected the samples are by signal noise. It can be seen that some samples are affected by relatively larger signal noise at some frequencies, such as samples at 4925 Hz. Two data sets are used as the input parameters of IWC and AWI, respectively. The first data set (complete data set) includes all measured displacements, while the second data set (incomplete data set) has 180 measured displacements with the exclusion of 20 measurement points near the ends of the beam. Fig. 18 and Fig. 19 show the complex wavenumbers obtained by IWC and AWI based on these two data sets, respectively. As can be seen in Fig. 18, IWC returns a better estimation of the complex wavenumbers when using the second data set, especially for the imaginary part of wavenumbers. This phenomenon is also observed in the IWC results studied in Section 3.1.1. The reason behind this phenomenon is that the energy associated with nearly evanescent waves is contained near structural discontinuities, such as force sources or boundaries, accounting for a small portion of the overall signal. Thus, discarding the displacements of measurement points at the structural discontinuities can reduce the effect of evanescent waves on the propagative wavenumber extraction, especially on the imaginary part of the wavenumber, which is associated with wave attenuation. It is also worth noting that the signal model of IWC does not contain the evanescent wave component. Thus the IWC itself cannot eliminate the effect of evanescent waves on the wavenumber extraction of propagating waves. However, The AWI signal model includes the evanescent wave component, and it can be used to extract propagative and evanescent wavenumbers with high resolution, as discussed in Section 3.1.1. Thus, AWI has the ability to reduce the influence of evanescent waves on propagative wavenumber identification to a certain degree. Fig. 19 shows that the accuracy of complex wavenumbers obtained by AWI is slightly improved when only samples from the far field are considered. In addition to eliminating the effect of evanescent waves, this is most likely also due to the exclusion of samples at both ends of the beam, which are typically more disturbed by signal noise. Furthermore, the accuracy of the imaginary part of the wavenumber extracted by AWI is higher than that of IWC. IWC does not seem to be adapted to extract the imaginary part of the wavenumber for low damping structures, and the same conclusion was also obtained by [7, 12, 38].

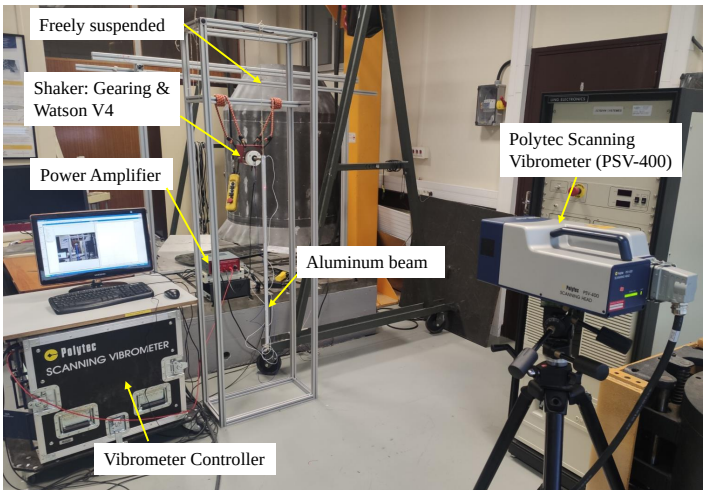


**Fig. 16.** Experiment set-up for measuring vibratory field of the aluminum beam

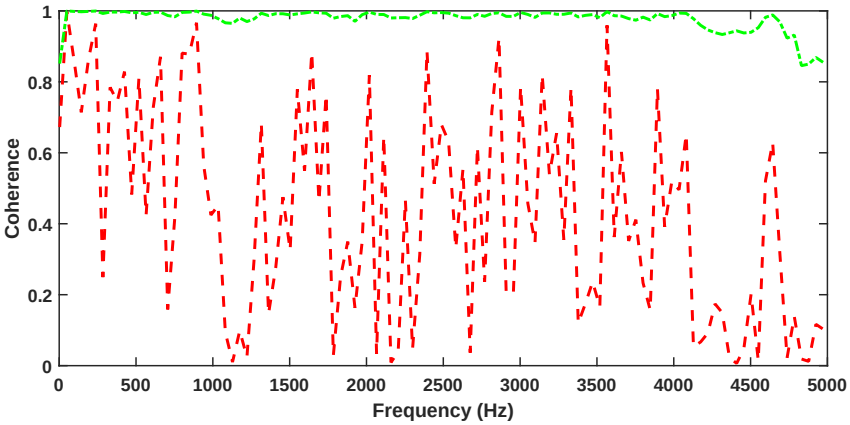


**Fig. 17.** Envelope of coherence function calculated for all measurement points. (– – –) minimum value of coherence function (—·—) maximum value of coherence function.

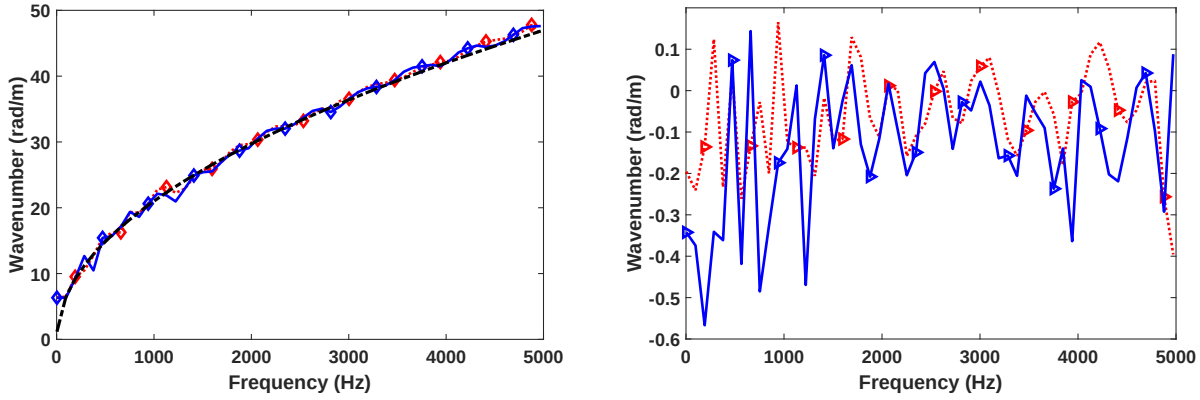


(a) (b)

**Fig. 18.** Comparison of wavenumber obtained by IWC using the complete and incomplete data set: (a) real part of wavenumber; (b) imaginary part of wavenumber. (◊—) real part of the wavenumber obtained by IWC using the complete data set, (▷—) imaginary part of the wavenumber obtained by IWC using the complete data set, (◊- - - - -) real part of the wavenumber obtained by IWC using the incomplete data set, (▷- - - - -) imaginary part of the wavenumber obtained by IWC using the incomplete data set, (—·—) real part of the wavenumber obtained by WFEM.

## 5. Conclusions

In this paper, Algebraic Wavenumber Identification (AWI) technique was developed based on the algebraic parameter estimator. The main contribution of AWI is that it can perform well on wavenumber extraction under different stochastic conditions, overcoming some known drawbacks of IWC and INCOME, which are the representative nonlinear family method and linear Prony family method, respectively. A comparison of the general properties between the proposed method and these two inverse methods is summarized in Table 4 wherein "Exact" refers to the ability to extract exact wavenumbers in the perfect condition and "uncertainty" refers to the small perturbation caused by uncertainty in geometric coordinates of measurement points. Additionally, INCOME is not adapted to extracting wavenumbers in periodic structures of unknown periodic length, while IWC and AWI do not have this limitation.

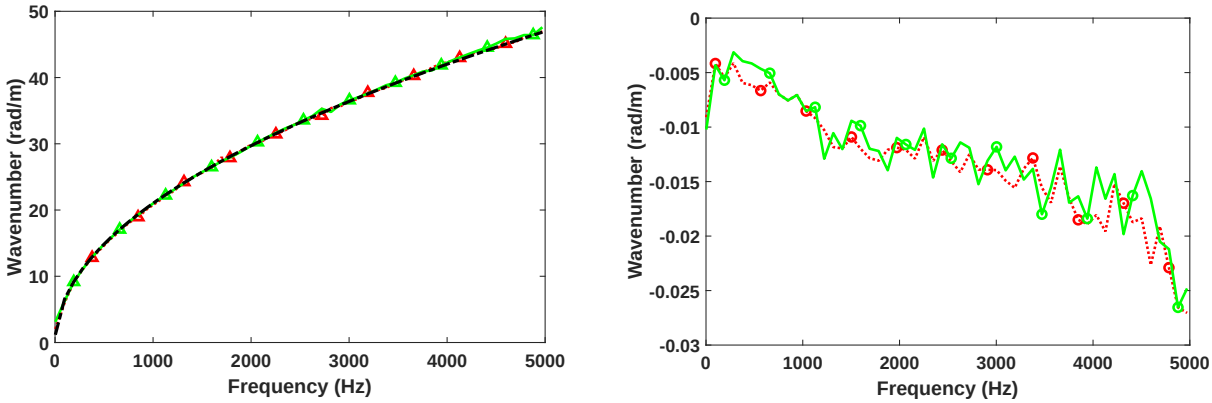


(a) (b)

**Fig. 19.** Comparison of wavenumber obtained by AWI using the complete and incomplete data set: (a) real part of wavenumber; (b) imaginary part of wavenumber. (△—) real part of the wavenumber obtained by AWI using the complete data set, (○—) imaginary part of the wavenumber obtained by AWI using the complete data set, (△ - - - - -) real part of the wavenumber obtained by AWI using the incomplete data set, (○- - - - -) imaginary part of the wavenumber obtained by AWI using the incomplete data set, (— · —) real part of the wavenumber obtained by WFEM.

**Table 4.** Comparison of general properties between IWC, INCOME, and AWI.

| Methods | Exact | Sampling limits | Computational time | Robust to signal noise | Robust to uncertainty | Frequency range |
|---|---|---|---|---|---|---|
| IWC | No | None | Time-consuming | Yes | Yes | Mid-High |
| INCOME | Yes | Periodicity | Efficient | No | No | All |
| AWI | Yes | None | Efficient | Yes | Yes | All |

In this work, three numerical cases are used to validate the ability of AWI to overcome the drawbacks of INCOME and IWC mentioned in Table 4. In the first numerical study, AWI, INCOME, and IWC are applied to a homogeneous aluminum beam under the perfect condition and signal noise condition. The results show that AWI is 5 to 8 times faster than IWC, and AWI is more robust than INCOME when samples are affected by the high level of signal noise. The second numerical study is investigated on a meta-structure to compare AWI and INCOME under small perturbation conditions and nonuniform sampling conditions. This numerical case illustrates that INCOME is sensitive to small perturbation and limited to periodic sampling, whereas AWI has a good performance in identifying wavenumber and band gap under these two stochastic conditions. Finally, the ability of AWI to extract complex wavenumber of periodic structures is validated when the structural periodicity is unknown through a bi-material periodic beam. Notably, the good performance of AWI can be attributed to three factors: a) The multiple integrals are introduced in the formula of AWI to improve its robustness to measurement errors; b) AWI treats the signal as a continuous function, resulting in the fact the AWI is not limited to periodic sampling and not sensitive to structural periodicity; c) The AWI algorithm only involves the several linear equations, reducing the computational cost compared to nonlinear family inverse methods, such as IWC.

In addition, AWI and IWC are applied to different experimental data sets of an aluminum beam. By means of this experimental study, two conclusions can be obtained: (a) the performance of AWI and IWC can be improved

when only using the samples which have a distance from the force source and boundaries as input parameters. This is because this sampling way can reduce the influence of the evanescent waves on the accuracy of extracted propagative wavenumbers; (b) AWI has the ability to reduce the influence of evanescent waves on propagative wavenumber extraction to a certain degree due to the fact that AWI can extract propagative wavenumbers and evanescent wavenumbers with high resolution.

For 2D applications, AWI needs to solve the problem with bivariate parameter extraction, which is the challenge of the algebraic parameter estimator. A forthcoming study should address the potential applicability of AWI concept to tackle 2D problems. Its performance on wavenumber identification of the plates has been validated by a series of numerical and experimental cases.

## Acknowledgements

This work is supported by the LabEx CeLyA (Centre Lyonnais d'Acoustique, ANR-10-LABX-0060) of Université de Lyon. The research of X. Li is funded by the China Scholarship Council (CSC).

## References

[1] M. I. Hussein, M. Leamy, M. J. Ruzzene, Dynamics of phononic materials and structures: Historical origins, recent progress, and future outlook, Applied Mechanics Reviews 66 (4) (2014) 040802. doi:https://doi.org/10.1115/1.4026911.

[2] R. Kumaresan, D. Tufts, Estimating the parameters of exponentially damped sinusoids and pole-zero modeling in noise, IEEE transactions on acoustics, speech, and signal processing 30 (6) (1982) 833–840. doi:https://doi.org/10.1109/TASSP.1982.1163974.

[3] M. R. Osborne, G. K. Smyth, A modified prony algorithm for exponential function fitting, SIAM Journal on Scientific Computing 16 (1) (1995) 119–138. doi:https://doi.org/10.1137/0916008.

[4] J. G. Mcdaniel, W. S. Shepard, Estimation of structural wave numbers from spatially sparse response measurements, Journal of the Acoustical Society of America 108 (4) (2000) 1674–82. doi:https://doi.org/10.1121/1.1310668.

[5] S. Rouquette, M. Najim, Estimation of frequencies and damping factors by two-dimensional esprit type methods, IEEE Transactions on signal processing 49 (1) (2001) 237–245. doi:https://doi.org/10.1109/78.890367.

[6] J. Berthaut, M. Ichchou, L. Jezequel, K-space identification of apparent structural behaviour, Journal of Sound and Vibration 280 (3-5) (2005) 1125–1131. doi:https://doi.org/10.1016/j.jsv.2004.02.044.

[7] C. Halkyard, Maximum likelihood estimation of flexural wavenumbers in lightly damped plates, Journal of sound and vibration 300 (1-2) (2007) 217–240. doi:https://doi.org/10.1016/j.jsv.2006.08.019.

[8] A. Geslain, S. Raetz, M. Hiraiwa, M. Abi Ghanem, S. Wallen, A. Khanolkar, N. Boechler, J. Laurent, C. Prada, A. Duclos, et al., Spatial Laplace transform for complex wavenumber recovery and its application to the analysis of attenuation in acoustic systems, Journal of Applied Physics 120 (13) (2016) 135107. doi:https://doi.org/10.1063/1.4963827.

[9] P. Margerit, A. Lebée, J.-F. Caron, X. Boutillon, High Resolution Wavenumber Analysis (HRWA) for the mechanical characterisation of viscoelastic beams, Journal of Sound and Vibration 433 (2018) 198–211. doi:https://doi.org/10.1016/j.jsv.2018.06.062.

[10] R. F. Boukadia, C. Claeys, C. Droz, M. Ichchou, W. Desmet, E. Deckers, An Inverse COnvolution MEthod for wavenumber extraction (INCOME): Formulations and applications, Journal of Sound and Vibration 520 (2022) 116586. doi:https://doi.org/10.1016/j.jsv.2021.116586.

[11] J. G. McDaniel, P. Dupont, L. Salvino, A wave approach to estimating frequency-dependent damping under transient loading, Journal of sound and vibration 231 (2) (2000) 433–449. doi:https://doi.org/10.1006/jsvi.1999.2723.

[12] M. Rak, M. Ichchou, J. Holnicki-Szulc, Identification of structural loss factor from spatially distributed measurements on beams with viscoelastic layer, Journal of Sound and Vibration 310 (4-5) (2008) 801–811. doi:https://doi.org/10.1016/j.jsv.2007.11.026.

[13] M. Ichchou, J. Berthaut, M. Collet, Multi-mode wave propagation in ribbed plates: Part i, wavenumber-space characteristics, International Journal of Solids and Structures 45 (5) (2008) 1179–1195. doi:https://doi.org/10.1016/j.ijsolstr.2007.09.032.

[14] M. Ichchou, O. Bareille, J. Berthaut, Identification of effective sandwich structural properties via an inverse wave approach, Engineering Structures 30 (10) (2008) 2591–2604. doi:https://doi.org/10.1016/j.engstruct.2008.02.009.

[15] R. Ajili, O. Bareille, M.-L. Bouazizi, M.-N. Ichchou, N. Bouhaddi, Parameter identification of a sandwich beam using numerical-based inhomogeneous wave correlation method, Advances in Acoustics and Vibration (2017) 65–75.doi:https://doi.org/10.1007/978-3-319-41459-1_7.

[16] G. Tufano, F. Errico, O. Robin, C. Droz, M. Ichchou, B. Pluymers, W. Desmet, N. Atalla, K-space analysis of complex large-scale metastructures using the inhomogeneous wave correlation method, Mechanical Systems and Signal Processing 135 (2020) 106407. doi:https://doi.org/10.1016/j.ymssp.2019.106407.

[17] R. Lajili, O. Bareille, M. L. Bouazizi, M. N. Ichchou, N. Bouhaddi, Composite beam identification using a variant of the inhomogeneous wave correlation method in presence of uncertainties, Engineering Computations 35 (6) (2018) 2126–2164. doi:https://doi.org/10.1108/EC-03-2017-0072.

[18] R. Lajili, K. Chikhaoui, Z. Zergoune, M.-L. Bouazizi, M.-N. Ichchou, Impact of the vibration measurement points geometric coordinates uncertainties on two-dimensional k-space identification: Application to a sandwich plate with honeycomb core, Mechanical Systems and Signal Processing 167 (2022) 108509. doi:https://doi.org/10.1016/j.ymssp.2021.108509.

[19] R. Prony, Essai éxperimental et analytique: sur les lois de la dilatabilité de fluides élastique et sur celles de la force expansive de la vapeur de l'alkool, à différentes températures, Journal de l'École Polytechnique Floréal et Plairial, an III 2 (1795) 24–76.

[20] P. Margerit, A. Lebée, J.-F. Caron, K. Ege, X. Boutillon, The high-resolution wavevector analysis for the characterization of the dynamic response of composite plates, Journal of Sound and Vibration 458 (2019) 177–196. doi:https://doi.org/10.1016/j.jsv.2019.06.026.

[21] L. Ribeiro, V. Dal Poggetto, B. Huallpa, J. Arruda, Bloch wavenumber identification of periodic structures using prony's method, Mechanical Systems and Signal Processing 178 (2022) 109242. doi:https://doi.org/10.1016/j.ymssp.2022.109242.

[22] R. Lajili, O. Bareille, M.-L. Bouazizi, M.-N. Ichchou, N. Bouhaddi, Inhomogeneous wave correlation for propagation parameters identification in presence of uncertainties, International Conference Design and Modeling of Mechanical Systems 5 (2017) 823–833. doi:https://doi.org/10.1007/978-3-319-66697-6_80.

[23] M. Fliess, R. Marquez, Continuous-time linear predictive control and flatness: a module-theoretic setting with examples, International Journal of Control 73 (7) (2000) 606–623. doi:https://doi.org/10.1080/002071700219452.

[24] M. Fliess, R. Marquez, E. Delaleau, H. Sira-Ramírez, Correcteurs proportionnels-intégraux généralisés, ESAIM: Control, Optimisation and Calculus of Variations 7 (2002) 23–41. doi:https://doi.org/10.1051/cocv:2002002.

[25] J.-P. Barbot, M. Fliess, T. Floquet, An algebraic framework for the design of nonlinear observers with unknown inputs, 2007 46th IEEE Conference on Decision and Control (2007) 384–389.doi:https://doi.org/10.1109/CDC.2007.4434695.

[26] M. Fliess, H. Sira-Ramirez, Closed-loop parametric identification for continuous-time linear systems via new algebraic techniques, Identification of Continuous-time Models from sampled Data (2008) 363–391.doi:https://doi.org/10.1007/978-1-84800-161-9_13.

[27] M. Fliess, H. Sira-Ramirez, An algebraic framework for linear identification, ESAIM: Control, Optimisation and Calculus of Variations 9 (2003) 151–168. doi:https://doi.org/10.1051/cocv:2003008.

[28] E. Pereira, J. R. Trapero, I. M. Díaz, V. Feliu, Algebraic identification of the first two natural frequencies of flexible-beam-like structures, Mechanical Systems and Signal Processing 25 (7) (2011) 2324–2335. doi:https://doi.org/10.1016/j.ymssp.2011.03.00.

[29] F. Beltrán-Carbajal, G. Silva-Navarro, Adaptive-like vibration control in mechanical systems with unknown paramenters and signals, Asian Journal of Control 15 (6) (2013) 1613–1626. doi:https://doi.org/10.1002/asjc.727.

[30] L. G. Trujillo-Franco, G. Silva-Navarro, F. Beltran-Carbajal, E. Campos-Mercado, H. F. Abundis-Fong, On-line modal parameter identifica-

tion applied to linear and nonlinear vibration absorbers, Actuators 9 (2020) 119. doi:https://doi.org/10.3390/act9040119.

[31] U. Lee, Spectral element method in structural dynamics, John Wiley & Sons, 2009. doi:10.1002/9780470823767.

[32] J. Mikusiński, T. K. Boehme, Operational calculus, vol. 1–2 (1983).

[33] A. P. Prudnikov, Operational calculus and related topics, Chapman and Hall/CRC, 2006. doi:10.1201/9781420011494.

[34] F. Beltran-Carbajal, G. Silva-Navarro, On the algebraic parameter identification of vibrating mechanical systems, International Journal of Mechanical Sciences 92 (2015) 178–186. doi:https://doi.org/10.1016/j.ijmecsci.2014.12.006.

[35] J. Havlík, O. Straka, U. D. Hanebeck, Stochastic Integration Filter: Theoretical and implementation aspects, 2018 21st International Conference on Information Fusion (FUSION) (2018) 1699–1706.doi:https://doi.org/10.23919/ICIF.2018.8455586.

[36] D. L. Carní, G. Fedele, Multi-sine fitting algorithm enhancement for sinusoidal signal characterization, Computer Standards & Interfaces 34 (6) (2012) 535–540. doi:https://doi.org/10.1016/j.csi.2011.03.003.

[37] A. Neves, M. D. Miranda, M. Mboup, Algebraic parameter estimation of damped exponentials, 2007 15th European Signal Processing Conference (2007) 965–969.

[38] R. Cherif, J.-D. Chazot, N. Atalla, Damping loss factor estimation of two-dimensional orthotropic structures from a displacement field measurement, Journal of sound and vibration 356 (2015) 61–71. doi:https://doi.org/10.1016/j.jsv.2015.06.042.